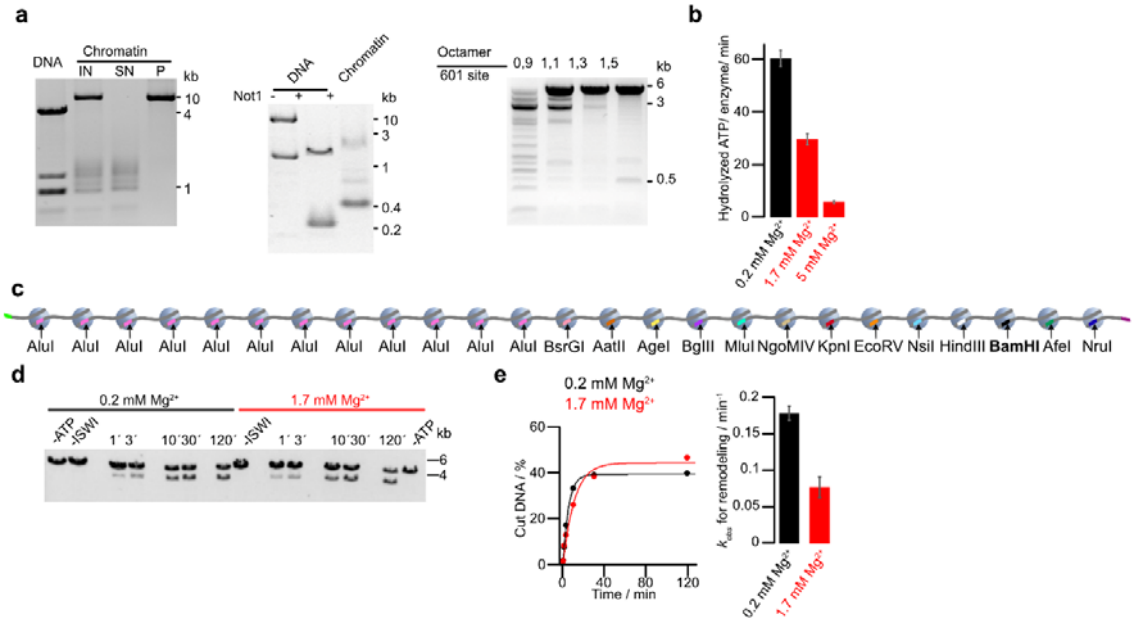

Figure S1. a, Quality controls for 25mer nucleosome arrays. Left: agarose gel after magnesium precipitation of assembled arrays and the resolubilized pellet. IN, input; SN, supernatant; P, pellet. Competitor DNA derived from the plasmid backbone (< 1 kb) was excluded from P. Middle: Not1 digestion (a Not1 site is present in each linker) liberated mostly mononucleosomes, running around 400 bp, but little 197 bp fragments, confirming saturation of most 601 repeats with octamers. Right: BsiWI digestion (all nucleosomes occlude a BsiWI restriction site) for arrays assembled with different octamer amounts. As 601 sites become saturated, digestion is hindered. **b**, ATP turnover in the presence of saturating concentrations of mononucleosomes (1.33 µM). Control experiments with three times lower mononucleosome concentrations gave the same results. Bars are mean values of two independent experiments, error bars their minimal and maximal values. Increasing Mg-concentrations reduce mononucleosome-stimulated ATP hydrolysis rates at saturating concentrations of ATP (1 mM). **c**, As in Fig. 1a, but with different orientation of the unique restriction sites such that the BamHI site is now more peripheral. **d**, BamHI accessibility assay as in Fig. 1f but for the array shown in *c*. **e**, Left: quantification of gel in *d* and exponential fits of time courses. Right: rate coefficients from single exponential fits. Bars are mean values of two independent experiments, error bars their minimal and maximal values.

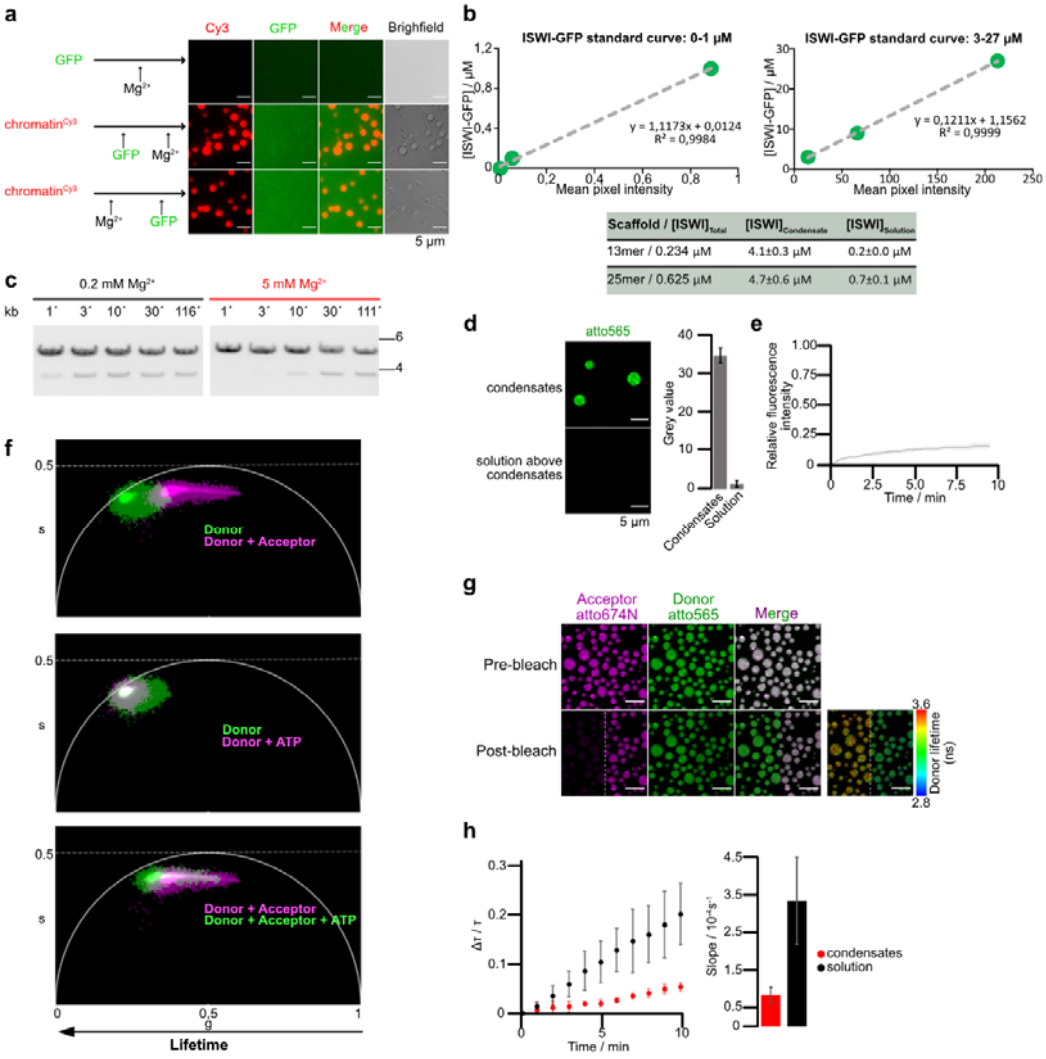

907

908 **Figure S2. a,** GFP does not partition into chromatin condensates. The colocalization experiment was
909 performed with 40 nM of unlabeled 25mer, 10 nM of 25mer-Cy3 and 1.125 µM of GFP-GST. **b,** ISWI-
910 GFP concentrations were determined inside condensates and, after centrifugation, in the surrounding
911 solution (bottom) from fluorescence intensities using calibration curves with ISWI-GFP dilutions (top).
912 Two different microscope settings were used to image lower and higher dilutions. Means and SD of
913 two independent replicates are shown. **c,** Nucleosome sliding time courses in absence and presence
914 of condensates (0.2 mM and 5 mM $MgCl_2$, respectively), replicate of experiment in Fig. 2e. Sliding was
915 measured by KpnI accessibility of 25mer arrays (15 nM). Reactions contained 750 nM ISWI and were
916 started by addition of 1 mM Mg-ATP. **d,** Enrichment of labeled 0N60 mononucleosomes in chromatin
917 condensates, N = 3 ± SD. The mononucleosome concentration in solution was determined from z-
918 plane above the condensates. **e,** Whole condensate FRAP of FRET-0N60 nucleosomes to assess their
919 exchange between condensate and solution. Line is an average and shadow SD of eight bleached
920 condensates. One of four independent replicates with similar results is shown. **f,** Phasor
921 representation of data in Fig. 2f. The phasor representation makes no assumptions on the number of
922 decay rates nor on specific decay model (exponential, non-exponential) (Digman et al., 2008). Upon

923 introduction of the acceptor, the donor's lifetime distribution moves away from the universal circle
924 line (single exponential lifetimes). This is consistent with an existence of at least two or even three
925 different populations of donor: high FRET, low FRET and no FRET. **g,** Acceptor bleaching enhances
926 donor fluorescence and lifetime, indicative of FRET. Imaging of FRET-0N60 nucleosomes in chromatin
927 condensates. The acceptor fluorophore was bleached in the left half of the field of view, leading to an
928 increase in donor fluorescence and donor lifetime (right most panel). **h,** FLIM-FRET measurements as
929 in Fig. 2h, but with 5 mM Mg-ATP. Means and SD of three independent experiments.

930

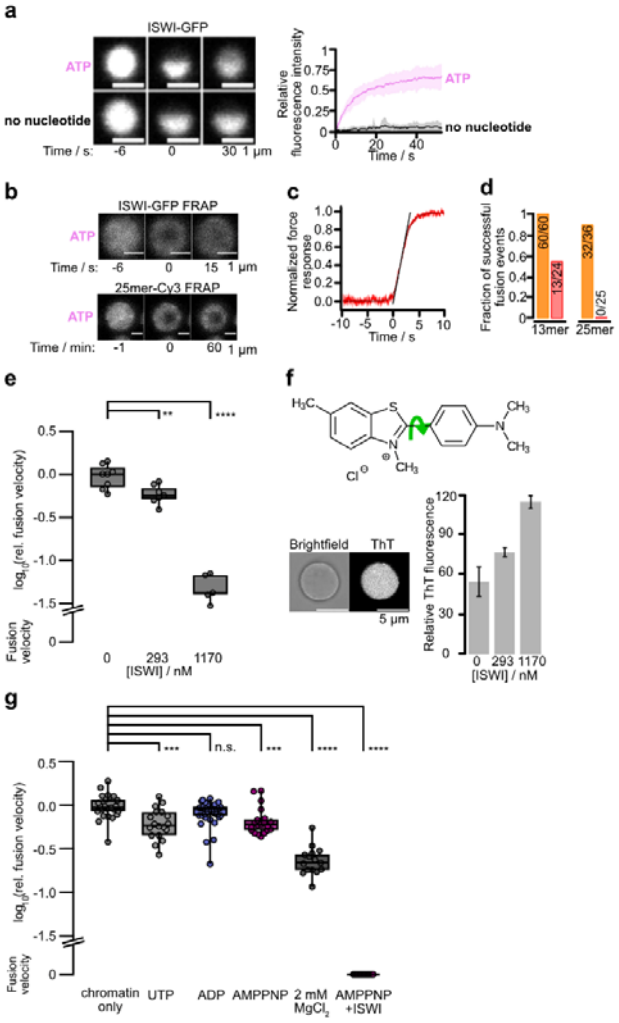

931

932 **Figure S3. a,** Intra-condensate mobility of ISWI-GFP measured by partial-condensate FRAP. Half of a
933 condensate was bleached in presence and absence of Mg-ATP (1 mM). Line is an average and shadow
934 SD of 15 bleached condensates for each condition. **b,** ISWI-GFP is more mobile than chromatin in
935 condensates. Dual FRAP of ISWI-GFP and Cy3-labeled condensates formed by 25mer arrays in
936 presence of Mg-ATP (1 mM) and ISWI (100 nM). Independent replicates show similar results. **c**, Force
937 readout of optical traps during controlled condensate fusion. The fusion velocity was determined as
938 the slope of the tangent fitted to the normalized force data at the inflection point of the fitted
939 function. Incurred forces during fusion are on the order of 1 pN (see Methods). **d,** Fraction of
940 successful fusion events in 1 mM $MgCl_2$ (orange) and 5 mM $MgCl_2$ (red). Total nucleosome
941 concentration was 1170 nM. **e,** Fusion between condensates measured by optical tweezers containing
942 indicated ISWI concentrations and 1170 nM nucleosomes. Velocities were estimated as illustrated in
943 Fig. S3c. Box plots show means and 25^{th}/75^{th} percentiles, whiskers the 9^{th} and 91^{st} percentiles. **f,** ISWI
944 increased viscosity of condensates as reported by enhanced fluorescence of the molecular rotor
945 thioflavin T (ThT). In a high viscosity medium, rotation around the C-C bond (green arrow) is
946 constrained, and the excitation energy is released as fluorescence. Bars are average ThT fluorescence
947 intensities relative to the outside medium; error: SD. Six condensates were analyzed for no ISWI and

293 nM ISWI, five for 1170 nM ISWI. **g**, Fusion between condensates without ISWI measured by optical tweezers. Nucleotides and free Mg^{2+} show only modest effects on fusion velocity.

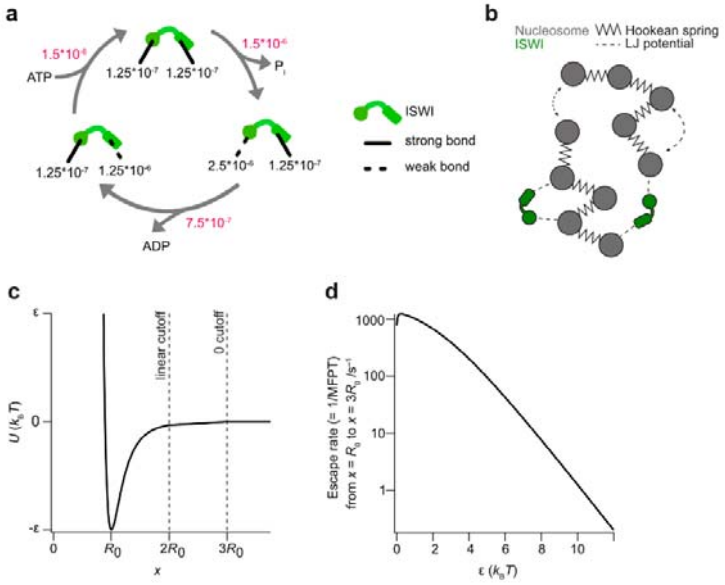

Figure S4. a, A model for the independent switching of the strengths of the two nucleosome interaction sites during ISWI´s ATPase cycle. Escape rates (black) and transition rates (red) in timestep^{-1} are indicated. **b,** Schematic representation of the implementation of the model in Fig. 4a for molecular dynamics simulations. **c,** Modified Lennard-Jones potential used in simulations. Below distances of $2R_0$ a regular Lennard-Jones potential is used. Between $2R_0$ and $3R_0$ the potential is described using a linear approximation, while interactions with range above $3R_0$ are set to 0. **d,** Conversion of the strength of the modified Lennard-Jones potential to escape rates based on the mean first passage time of potential escape (Gray & Yong, 2021).

Movie S1. FLIM-FRET timelapse with ATP

Movie S2. FLIM-FRET timelapse with AMPPNP

Movie S3. Controlled fusion with optical tweezers of chromatin condensates containing ISWI and ADP-BeF$_x$

Movie S4. Controlled fusion with optical tweezers of chromatin condensates containing ISWI and ATP

Movie S5. Simulation of ISWI FRAP with graph

966 **Movie S6. Simulation of condensate fusion with graph**

967 **Table S1. Oligonucleotide list**

Name	Sequence (5'->3')	Description
oFMP839	GCTTGCATGCCTGCAGGTCG	To PCR ON60 fragment used for ATPase assay
oFMP864	CTGGAGAATCCCGGTGCCG	To PCR ON60 fragment used for ATPase assay and 0N60-EcoRI fragment used for FLIM-FRET
oFMP1260	TAAGCAGAATTCGCTTGCATGCCTGCAGGTCG	To PCR [atto647N]0N60-EcoRI fragment used for FLIM-FRET
oFMP1261	[ATTO647N]CTGGAGAATCCCGGTGCCG	To PCR [atto647N]0N60-EcoRI fragment used for FLIM-FRET and 0N60-EcoRI fragment used for FLIM-FRET

968